Concentration Polarization in Stirred Ultrafiltration Cells

Scott T. Johnston and Kenneth A. Smith
Dept. of Chemical Engineering, Massachusetts Institute of Technology, Cambridge, MA 02139

William M. Deen
Dept. of Chemical Engineering and Div. of Bioengineering and Environmental Health, Massachusetts Institute of Technology, Cambridge, MA 02139

Laminar boundary-layer theory was used to quantify concentration polarization in ultrafiltration systems in which the membrane forms the base of a stirred, cylindrical container. The flow was approximated as a rigid-body rotation above a stationary surface (Bödewadt flow), with a filtration velocity dependent on the osmotic pressure of the retained solute, and therefore varying with radial position on the surface. Because the analysis was limited to moderate solute concentrations and filtrate velocities, physical properties were assumed to be constant. The axisymmetric convective-diffusion problem was solved by a finite difference method. Boundary-layer results were compared with predictions based on the common assumption of a uniform stagnant film and with a hybrid approach of applying locally the stagnant-film relationships but allowing the film thickness to vary with position. In general, both of the approximate models underestimated polarization effects, with the hybrid approach yielding smaller errors. In one set of simulations on the osmotic reduction in filtration rate caused by a completely retained solute, predicted errors in filtration rates with the models were moderate, with a maximum discrepancy of 21% (for the stagnant-film model). In the second set of simulations concerning polarization effects on apparent sieving coefficients for permeable solutes, the error in the predicted ratio of true-to-observed sieving coefficient was as much as 78% with the stagnant-film approach, while with the hybrid model it was no more than 15%. Thus, the stagnant-film approach was much less satisfactory for inferring sieving coefficients than for predicting mean filtrate velocities. The predictive capability of the boundary-layer model was tested using previous filtration data for bovine serum albumin in two ultrafiltration cells. The agreement was excellent, provided that an appropriate value was selected for the angular velocity of the bulk fluid.

Introduction

A well-known phenomenon in ultrafiltration, termed *concentration polarization*, is the tendency of retained solutes to accumulate near the upstream surface of a membrane. High solute concentrations at the membrane surface reduce filtration rates (either osmotically or by surface blockage), and also tend to increase solute passage through the membrane. Thus, concentration polarization both degrades separations and complicates efforts to use sieving measurements to characterize membranes.

The simplest description of concentration polarization is derived from a stagnant-film model, used by Sherwood et al. (1965) to analyze reverse osmosis and first applied to ultrafiltration by Michaels (1968). The stagnant-film model has been used in many subsequent ultrafiltration studies (Opong and Zydney, 1991; Zydney, 1997; Johnston and Deen, 1999). In this approach, attention is focused on a thin layer of fluid next to the membrane, and a one-dimensional problem is ob-

Correspondence concerning this article should be addressed to W. M. Deen.

tained by assuming that the solute concentration depends only on distance from the membrane surface. Only convection and diffusion normal to the membrane are considered explicitly. The effects of convective transport parallel to the membrane surface are embedded in the value of the effective film thickness (δ). The analytical solution to this one-dimensional problem yields an expression for what we term the *polarization factor* (B),

$$B \equiv \frac{C_m - C_f}{C_b - C_f} = \exp\left(\frac{v_f}{k_{sf}}\right), \tag{1}$$

where C_m, C_f, and C_b are concentrations at the membrane surface, in the filtrate, and in the bulk retentate solution, respectively, and v_f is the filtrate velocity (that is, the volume flux relative to the membrane). The mass-transfer coefficient for the stagnant-film model (k_{sf}) is related to the solute diffusivity (D) and film thickness by $k_{sf} = D/\delta$. Equation 1 captures the essential feature of concentration polarization, which is that it is worsened as v_f/k_{sf} is increased. Only for $v_f/k_{sf} \to 0$ does $B \to 1$, indicating that polarization is negligible.

Equation 1 is attractive because of its simplicity, but its predictive ability is limited by the unknown nature of δ for many systems. Although δ can be estimated from experimental information on the mass-transfer coefficient for a given solute and a given filtration rate, there is no guarantee that the same value of δ will be applicable to other conditions, as one might hope. Indeed, a recent analysis of ultrafiltration data for bovine serum albumin (BSA) solutions in small stirred cells yielded apparent values of k_{sf} (and hence δ) that were quite sensitive to v_f (Johnston and Deen, 1999). Moreover, even for mass transfer in systems without filtration, scaling arguments based on laminar boundary-layer theory show that effective film thicknesses must vary with D (Deen, 1998, p. 422).

More rigorous analyses of concentration fields in ultrafiltration are complicated by the fact that such problems are usually made nonlinear by the dependence of v_f on the solute concentration. That is, the osmotic pressure opposing filtration is determined by the solute concentration at the upstream membrane surface. Unless the osmotic pressure is much smaller than the applied transmembrane pressure, this precludes attempts to compute the velocity field without simultaneously addressing the mass-transfer problem. In concentrated solutions, the complexity may be exacerbated by variable viscosities and/or diffusivities. Nonetheless, detailed analyses are available for certain geometries. A number of authors have computed two-dimensional concentration fields for laminar cross-flow ultrafiltration in tubes or parallel-plate channels (Shen and Probstein, 1977; Gill et al., 1988; Denisov, 1994; Bhattacharjee et al., 1999). Other systems for which there have been detailed analyses include spiral-wound membrane modules (Madireddi et al., 1999) and two-dimensional stagnation flow (Kozinski and Lightfoot, 1971). Some authors have employed a ''hybrid'' approach, which applies the stagnant-film model locally, in combination with theoretical information on mass-transfer coefficients in the absence of filtration. This approach, which has been applied mainly to cross-flow systems, avoids having to assume that δ is spatially uniform and thereby allows v_f and C_m to vary with position (Blatt et al., 1970; Zydney, 1997). The hybrid approach is implemented most readily when a simple expression is available for the mass-transfer coefficient, as in the entrance region of a tube or parallel-plate channel.

Systems in which the membrane forms the base of a stirred cylindrical cell are often used experimentally, but have received relatively little theoretical attention. In what appears to be the only detailed analysis of convective diffusion in this type of ultrafiltration system, Saksena and Zydney (1997) approximated the flow as a rigid-body rotation above a stationary surface (known as Bödewadt flow), and included filtration by superimposing on the main flow a small velocity normal to the surface. A very similar fluid dynamical model was used by Smith and Colton (1972), who analyzed mass transfer to the base of a stirred cylindrical container in the absence of filtration (e.g., a dialysis cell). For the ultrafiltration problem, Saksena and Zydney used a similarity transformation to reduce the axisymmetric species conservation equation to an ordinary differential equation, which was solved numerically. This transformation was made possible by assuming that the product of $v_f(r)$ and the concentration boundary layer thickness was a constant, where r is the radial position. Although not emphasized by those authors, it also was necessary that the filtrate concentration be independent of the radial position. The main objective of that work was to examine the effects of solute–solute diffusional interactions in concentrated solutions, but the same assumptions would be required to apply the similarity transformation to dilute solutions. Those approximations limit the generality of that approach.

The purpose of the present study was to investigate further the Bödewadt flow model for stirred-cell ultrafiltration. By solving the axisymmetric species conservation equation numerically, restrictions on the radial variations of v_f and filtrate concentration were avoided. The analysis is limited to laminar flow at high Reynolds number and high Schmidt number. [In stirred cells the transition from laminar to turbulent flow occurs at a Reynolds number of approximately 3×10^4 (Colton and Smith, 1972), and Schmidt numbers for protein solutions are typically $> 10^4$.] Solute concentrations were assumed to be moderate, as is typical of membrane characterization experiments, allowing the viscosity and diffusivity to be regarded as constants. The boundary-layer formulation and solution methods are described first. Then, certain general results are discussed in comparison with predictions of stagnant-film and hybrid models. Finally, the predictions of the boundary-layer model are tested using previously reported data on the filtration of BSA solutions in commercial ultrafiltration cells (Johnston and Deen, 1999).

Model Development

Overview

The system of interest is depicted in Figure 1a. An ultrafiltration membrane forms the base of a cylindrical cell of radius R. The cell is partially filled with a macromolecule solution, which is stirred by an impeller that rotates at an angular velocity ω_s. A desired filtration rate is set by controlling the gas pressure, and the liquid volume is assumed to be sufficiently large that the process is pseudosteady. This system was modeled as shown in Figure 1b, in which a semi-infinite

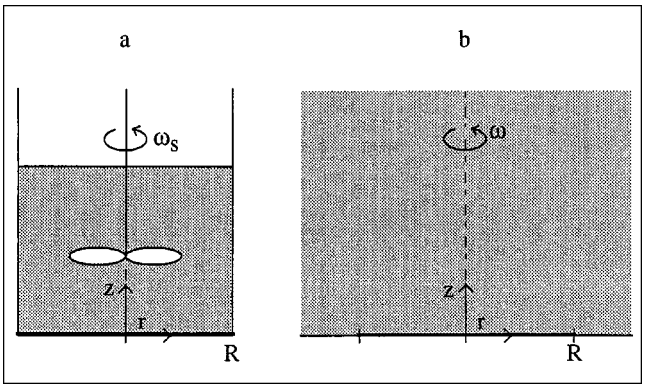

Figure 1. Flow in a typical stirred ultrafiltration cell (panel a) modeled as a semiinfinite fluid rotating above a surface (panel b).

The membrane radius is R. The angular velocity of the stirrer (ω_s) differs from that of the bulk fluid in the model (ω).

solution rotates above a stationary surface, with the angular velocity of the bulk liquid (which undergoes rigid-body rotation) denoted as ω. This representation was motivated by the fact that rotational flow above an impermeable, planar surface Bödewadt flow) has been well characterized (Schlicting, 1979, p. 225–230; Rogers and Lance, 1960), and the observation that those velocity results are readily modified to include moderate rates of filtration (Saksena and Zydney, 1997). In the model the membrane is considered to occupy a circular area of radius R within a larger surface. Because the stirrer must overcome the torques exerted on the fluid by the side and bottom of the cell, the rotation rate of the stirrer must exceed that of the bulk fluid; that is, $\omega/\omega_s < 1$, as will be seen in the discussion of the experimental results.

The omission of the impeller from the model system (Figure 1b) is justified by the fact that the momentum and concentration boundary-layer thicknesses in such systems are often much smaller than the impeller–surface separation. For laminar flow at high Reynolds number (Re), the momentum boundary-layer thickness (δ_m) is expected to scale as

$$\frac{\delta_m}{R} \sim Re^{-1/2}, \tag{2}$$

where $Re = \omega R^2/\upsilon$ and υ is the kinematic viscosity (Deen, 1998, p. 338). If the Schmidt number ($Sc = \upsilon/D$) is also large, the concentration boundary layer thickness (δ_c) will vary as

$$\frac{\delta_c}{R} \sim Re^{-1/2} Sc^{-1/3} \tag{3}$$

(Deen, 1998, p. 424). Thus, even for $Re = 10^3$ and $Sc = 10^4$, which are not particularly large values for protein solutions in stirred cells, δ_c would be only about 0.1% of R. This indicates that it is sufficient to focus on the region very near the membrane surface. The pressure and velocity fields in this thin region are discussed next, followed by a description of the convective diffusion problem.

Pressure field

It was assumed that the dynamic pressure in the liquid ($\mathcal{P}$) is approximately that for a fluid undergoing rigid-body rotation,

$$\mathcal{P}(r) = \frac{1}{2}\rho\omega^2 r^2, \tag{4}$$

where ρ is density. Here the arbitrary constant in the dynamic pressure was chosen so that $\mathcal{P} = 0$ at $r = 0$. The radial variation in pressure described by Eq. 4, when imposed on the boundary layer, results in a flow near the membrane that is directed inward (that is, toward the axis of rotation). It follows that the concentration boundary layer begins to develop at the outer edge of the membrane ($r = R$).

To calculate the filtrate velocity, an expression also was needed for the transmembrane pressure difference. Adding static pressure variations to those in Eq. 4, the actual liquid pressure (P) was found to be

$$P(r, z) = \mathcal{P}(r) - \rho g z + c = \frac{1}{2}\rho\omega^2 r^2 - \rho g z + c. \tag{5}$$

The constant c was determined by returning to the system in Figure 1a, equating pressures at the gas–liquid interface, and specifying the total volume of liquid. This was sufficient to define the height of the gas–liquid interface, which was found to be parabolic in r with a minimum at the center. The transmembrane pressure difference (ΔP) was then evaluated as

$$\Delta P \equiv P(r,0) - P_f = P_0 - P_f + \rho g h_0 + \frac{1}{2}\rho\omega^2 R^2\left[\left(\frac{r}{R}\right)^2 - \frac{1}{2}\right], \tag{6}$$

where P_0 is the gas pressure, h_0 is the liquid height under static conditions, and P_f is the pressure in the filtrate (assumed constant). The last term in Eq. 6 is usually a small fraction of ΔP, so that in all simulations ΔP was assumed to be independent of r. For the experimental conditions discussed later, it was calculated that the radial variation in ΔP never exceeded 0.6% of its mean value.

Velocity field

The equations of motion for this system can be reduced to a set of ordinary differential equations by assuming a solution of the form

$$\upsilon_r = r\omega F(\zeta), \quad \upsilon_\theta = r\omega G(\zeta), \quad \upsilon_z = \sqrt{\upsilon\omega}\, H(\zeta) - \upsilon_f(r) \tag{7}$$

where $\upsilon_f(r)$ is the local velocity normal to the membrane surface (> 0 for filtration) and

$$\zeta \equiv z\sqrt{\frac{\omega}{\upsilon}}. \tag{8}$$

The dimensionless axial coordinate ζ is of order unity at the edge of the momentum boundary layer (Rogers and Lance, 1960). The inclusion of υ_f as an additive term in υ_z follows

Saksena and Zydney (1997). Using primes to denote derivatives with respect to ζ, the continuity equation becomes

$$H' + 2F = 0 \tag{9}$$

and the r- and θ-components of the Navier-Stokes equation transform to

$$F'' - F^2 + G^2 - HF' + \frac{v_f(r)}{\sqrt{v\omega}}F' = 1 \tag{10}$$

$$G'' - 2FG - HG' + \frac{v_f(r)}{\sqrt{v\omega}}G' = 0. \tag{11}$$

The z-component of the Navier-Stokes equation is not needed in this boundary-layer formulation. The boundary conditions that express no slip at the membrane surface, $v_z = -v_f$ at the surface, and rigid-body rotation far from the surface, are

$$F(0) = G(0) = H(0) = 0, \quad F(\infty) = 0, \quad G(\infty) = 1. \tag{12}$$

Equations 9–12 reduce to those applicable in the absence of filtration, provided that

$$\frac{v_f(r)}{\sqrt{v\omega}} \ll 1. \tag{13}$$

Therefore, if Eq. 13 is satisfied, previous results for $F(\zeta)$, $G(\zeta)$, and $H(\zeta)$ can be used for the filtration problem. [The functions defined here as $F(\zeta)$, $G(\zeta)$, and $H(\zeta)$ are those denoted in Rogers and Lance (1960) as $\mathfrak{F}(\xi)$, $\mathfrak{G}(\xi)$, and $\mathfrak{H}(\xi)$, respectively. In their analysis the bulk fluid and the surface were assumed to have angular velocities ω and $\sigma\omega$, respectively, so that Bödewadt flow corresponds to their special case of $\sigma = 0$.] Equation 13 is not difficult to satisfy; for the experiments discussed later, $\langle v_f \rangle / \sqrt{v\omega} \sim 10^{-4}$, where $\langle v_f \rangle$ is the filtrate velocity averaged over the membrane surface.

The thinness of the concentration boundary layer, relative to the momentum boundary layer, allowed us to simplify the velocity field by using expressions valid for small ζ. Thus, $F(\zeta)$ was approximated by its Maclaurin series expansion,

$$F(\zeta) = F'(0)\zeta + \frac{1}{2}F''(0)\zeta^2 + \cdots, \tag{14}$$

where we have used the fact that $F(0) = 0$. From Rogers and Lance (1960), $F'(0) = -0.94197$, indicating that the radial flow near the surface is directed inward, as already mentioned. [Following Eq. 21 of Saksena and Zydney (1997), the constant 0.94197 is given incorrectly as 0.525.] By fitting a curve to other results for $F(\zeta)$ tabulated in Schlichting (1979, p. 228), with the values of $F(0)$ and $F'(0)$ fixed as just described, it was found that $F''(0) = 1.10$. From continuity (Eq. 9), $H(\zeta)$ was expressed as

$$H(\zeta) = -F'(0)\zeta^2 - \frac{1}{3}F''(0)\zeta^3 + \cdots. \tag{15}$$

An expression for $G(\zeta)$, the dimensionless angular velocity, was not needed to compute the axisymmetric concentration field.

The filtration velocity was calculated from the transmembrane pressure drop and the osmotic pressure difference ($\Delta\Pi$) using

$$v_f = L_p(\Delta P - \sigma\Delta\Pi), \tag{16}$$

where L_p is the membrane hydraulic permeability and σ is the reflection coefficient. As discussed later, $\Delta\Pi$ was related to the solute concentration by using either the Van't Hoff equation or certain empirical expressions.

Concentration field

The steady, axisymmetric species conservation equation for the stirred cell is

$$v_r\frac{\partial C}{\partial r} + v_z\frac{\partial C}{\partial z} = D\left[\frac{\partial^2 C}{\partial z^2} + \frac{1}{r}\frac{\partial}{\partial r}\left(r\frac{\partial C}{\partial r}\right)\right], \tag{17}$$

where $C(r, z)$ is the solute concentration. The boundary conditions used were

$$C(R, z) = C_b \tag{18}$$

$$\frac{\partial C}{\partial z}(r, \infty) = 0 \tag{19}$$

,

$$\frac{\partial C}{\partial z}(r, 0) = -\frac{v_f(r)}{D}(1 - \Theta)C(r, 0), \tag{20}$$

where $\Theta = C_f(r)/C(r, 0)$ is the local value of the membrane sieving coefficient. Equation 18 requires that the concentration at the outer edge of the membrane (the ''leading edge'' for the concentration boundary layer) equal the bulk concentration. Equation 19 specifies that axial gradients in concentration vanish in the bulk solution, far from the surface. Equation 20 was derived by equating the axial flux at the membrane surface with the flux of solute in the filtrate.

In all of the present calculations Θ was regarded as a constant. Thus, to the extent that the concentration at the upstream membrane surface varied with radial position, the filtrate concentration did also. In general, for a given membrane–solute combination, Θ will depend on v_f. The constancy of Θ requires either that v_f be constant or that the membrane Péclet number be large (Deen, 1998, p. 67).

The species conservation equation was made dimensionless by introducing the following quantities:

$$Y = 1 - \frac{r}{R} \tag{21}$$

$$Z = Sc^{1/3}\zeta = Sc^{1/3}z\sqrt{\frac{\omega}{v}} \tag{22}$$

$$\Psi = \frac{C}{C_b} \tag{23}$$

$$\alpha(Y) = \frac{v_f(Y)}{\sqrt{v\omega}}Sc^{2/3}. \tag{24}$$

The reversed radial coordinate (Y) is a natural choice for this problem, because the concentration boundary layer grows

as one moves inward from the outer edge of the membrane. The new axial coordinate (Z) is scaled for the concentration boundary layer; that is, it is of order unity within that region. The function $\alpha(Y)$ is a dimensionless filtration rate, scaled as shown by $Sc^{2/3}$ in order to remove the Schmidt number from the boundary condition at the membrane surface. Substitution of these variables and the expansions for v_r and v_z in Eq. 17 gives

$$-(1-Y)\left[F'(0)Z+\frac{1}{2}F''(0)Z^2Sc^{-1/3}\right]\frac{\partial\Psi}{\partial Y}-\left[F'(0)Z^2+\frac{1}{3}F''(0)Z^3Sc^{-1/3}+\alpha(Y)\right]\frac{\partial\Psi}{\partial Z}=\frac{\partial^2\Psi}{\partial Z^2}+\frac{1}{ReSc^{2/3}}\left[\frac{\partial^2\Psi}{\partial Y^2}-\frac{1}{(1-Y)}\frac{\partial\Psi}{\partial Y}\right]. \quad (25)$$

Because the present analysis was restricted to the case of high *Re* and *Sc*, the radial diffusion term in Eq. 25 was neglected. Preliminary calculations revealed that for the large values of *Sc* of interest here ($>10^4$), the $F''(0)$ terms in the velocity components had a negligible effect on the model results. For example, for $Sc=1.5\times10^4$, inclusion of these higher-order terms resulted in $<0.5\%$ changes in both the area-averaged mass-transfer coefficient and the area-averaged surface concentration calculated by the model. Accordingly, Eq. 25 was simplified to

$$-(1-Y)F'(0)Z\frac{\partial\Psi}{\partial Y}-\left[F'(0)Z^2+\alpha(Y)\right]\frac{\partial\Psi}{\partial Z}=\frac{\partial^2\Psi}{\partial Z^2}. \quad (26)$$

The boundary conditions for $\Psi(Y,Z)$ are

$$\Psi(0,Z)=1 \quad (27)$$

$$\frac{\partial\Psi}{\partial Z}(Y,\infty)=0 \quad (28)$$

$$\frac{\partial\Psi}{\partial Z}(Y,0)=-\alpha(Y)[1-\Theta]\Psi(Y,0). \quad (29)$$

Note that with the scaling employed, which is valid asymptotically for large *Sc*, neither *Re* nor *Sc* appears in Eqs. 26–29. Thus, Ψ is dependent only on position (Y,Z) and the parameter α.

The local mass-transfer coefficient is defined as

$$k\equiv-\frac{D}{(C_m-C_b)}\left.\frac{\partial C}{\partial z}\right|_{z=0}, \quad (30)$$

so that it represents the diffusive portion of the solute flux. Given the functional dependence of Ψ and the relationship between Z and z (Eq. 22), it follows that the local Sherwood number is of the form

$$Sh=\frac{kR}{D}=f(Y,\alpha)Re^{1/2}Sc^{1/3}, \quad (31)$$

where the coefficient $f(Y,\alpha)$ is computed from the values of Ψ and $\partial\Psi/\partial Z$ at $Z=0$. In general, those results must be obtained numerically. However, for the region near the outer edge of the membrane and for small filtration rates, a useful analytical solution can be found. That solution (using similarity) is described next, and then the numerical procedure is outlined.

Similarity solution near membrane outer edge

As pointed out in Smith and Colton (1972), at the outer edge of the membrane axial convection is negligible for $\alpha=0$. This suggests that for $Y\ll1$ and $\alpha\to0$, Eq. 26 can be approximated as

$$-F'(0)Z\frac{\partial\Psi}{\partial Y}=\frac{\partial^2\Psi}{\partial Z^2}. \quad (32)$$

This is also a valid approximation for α of order one, provided that $Y^{1/3}\ll1$. For $\alpha\to0$ and a fixed value of Θ, Eq. 29 also reduces to a simpler form, corresponding to specification of a constant value of $\partial\Psi/\partial Z$ at the membrane surface. For the calculation of mass-transfer coefficients, the magnitude of that constant is immaterial. Thus, the simplified boundary condition at the membrane surface was written as

$$\frac{\partial\Psi(Y,0)}{\partial Z}=-1. \quad (33)$$

The other boundary conditions, given by Eqs. 27 and 28, remain the same. This problem was solved by assuming that $\Psi=\Psi(s)$ only, where

$$s\equiv Z\left(-\frac{9Y}{F'(0)}\right)^{-1/3}. \quad (34)$$

Using this similarity solution, the coefficient in the expression for the Sherwood number was found to be

$$f(Y,0)=\Gamma(2/3)\left[\frac{-F'(0)}{9}\right]^{1/3}Y^{-1/3}=0.6381Y^{-1/3}\quad(Y\ll1). \quad (35)$$

Numerical solution

The ''complete'' problem, that given by Eqs. 26–29, was solved using a modified Crank-Nicolson method. For simulations involving dilute solutions it was assumed that $\Delta\Pi=0$, making v_f a constant that could be specified in advance. With v_f independent of the concentration field, the latter could be computed in one step. For more concentrated solutions ($\Delta\Pi$ not negligible), an iterative procedure was required. An initial guess of a constant filtration rate was entered, and the concentration field was computed using this initial v_f. The osmotic pressure at the membrane surface was then calculated, and Eq. 16 was used to update $v_f(r)$ for use in the next iteration. The filtration rate was updated according to

$$v_f^{i+1}=v_f^i+f\left\{v_f\left[C^i(r,0)\right]-v_f^i\right\}, \quad (36)$$

where the superscripts indicate the iteration. Depending on the value chosen for the ''relaxation factor'' f in Eq. 36, the filtration rate used in iteration $i+1$ was somewhere between

that used in iteration i and that calculated from the concentration profile determined by iteration i. Iteration continued until the area-averaged filtration rate converged to within a relative tolerance of $<10^{-5}$. For most simulations $f = 0.5$ was sufficiently small to ensure convergence.

To accommodate a finite grid, the boundary condition at $Z = \infty$ (Eq. 28) was usually imposed at $Z = 10$. Increasing this value to 20 resulted in only a 0.5% change in the average surface concentration calculated by the model, confirming that 10 was sufficiently large. A 100×100 grid was found to provide results for the average surface concentration that were accurate to within 0.1%.

Results and Discussion

Mass-transfer coefficient

Smith and Colton (1972) investigated the problem of mass transfer in Bödewadt flow in the absence of filtration. They included radial diffusion, and computed the steady-state solution as the large-time limit of a transient problem, using an alternating-difference implicit procedure. Three types of boundary conditions were considered. The present results were compared with those of Smith and Colton by setting $\alpha(Y) = 0$ in Eq. 26 and replacing Eq. 29 with a constant concentration condition. For $Re = 10^4$ and $Sc = 10^5$, the two sets of mass-transfer coefficients were indistinguishable in the range $0 \le Y \le 0.97$. The present model did not allow calculation of mass-transfer coefficients for larger values of Y, due to instabilities in the concentration field that appeared as $Y \to 1$. A likely reason for failure of the numerical solution in this region is that the radial convection term in Eq. 26 vanishes, so that the partial differential equation loses its parabolic character. It also should be noted that the present formulation becomes inaccurate for $Y \to 1$, because the neglect of radial diffusion makes it impossible to impose the symmetry condition at the axis of rotation, namely, $\partial \Psi / \partial Y = 0$ at $Y = 1$. The numerical difficulties notwithstanding, it was possible in all simulations to obtain stable concentration values over 99.9% of the membrane area.

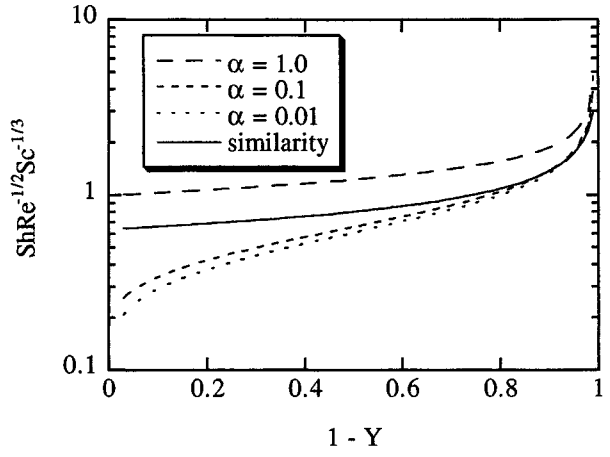

Figure 2. Dimensionless mass-transfer coefficient as a function of radial position.

Results from the boundary-layer model are shown for several values of the dimensionless filtration rate (α), with $\Theta = 0$ in each case. The curve labeled "similarity" was calculated from Eq. 35.

The behavior of the local mass-transfer coefficient was investigated using several constant values of the dimensionless filtration rate, α. (As noted earlier, α is constant when osmotic effects are negligible.) The results are plotted in Figure 2 as $Sh\, Re^{-1/2}\, Sc^{-1/3}$ vs. dimensionless radial position. Shown for comparison is the similarity result given by Eq. 35. In all cases, there was a rapid decline in mass-transfer coefficient when moving inward from the outer edge of the membrane, a consequence of the increasing thickness of the concentration boundary layer (see below). For a given radial position, the mass-transfer coefficient decreased as the filtration rate was reduced. The asymptotic limit reached for $\alpha \to 0$ was in excellent agreement with the similarity solution for the outer 10–15% of the membrane radius. The results for $\alpha = 0.001$ (not shown) were indistinguishable on this plot from those for $\alpha = 0.01$. As shown in Figure 2, the agreement with the analytical result was much worse for $\alpha = 1$. For filtration rates of that magnitude, the region in which axial convection may be neglected is much smaller ($Y^{1/3} \ll 1$).

Concentration field

Concentration contours representative of the behavior at moderate filtration rates are plotted in Figure 3. These calculations were performed for an ideal semipermeable membrane (that is, $\sigma = 1$ in Eq. 16 and $\Theta = 0$ in Eq. 29) and assumed that $\Pi \propto C$, as in the Van't Hoff equation. Under these conditions the only remaining dimensionless parameters are

$$\alpha_0 \equiv \frac{v_{f_0}}{\sqrt{v\omega}} Sc^{2/3} = \frac{L_p(\Delta P - \Pi_b)}{\sqrt{v\omega}} Sc^{2/3} \tag{37}$$

$$\beta \equiv \frac{\Pi_b}{\Delta P}, \tag{38}$$

where v_{f_0} and Π_b are the filtration velocity and osmotic pressure, respectively, based on the bulk solution concentration. The parameter α_0 is a scaled filtration velocity, and β is a measure of the importance of osmotic effects. For the results shown in Figure 3, $\alpha_o = 1$ and $\beta = 0.5$. As seen, each concentration contour had an inflection point. Taking the $\Psi = 1.01$ contour as an index of the boundary-layer thickness,

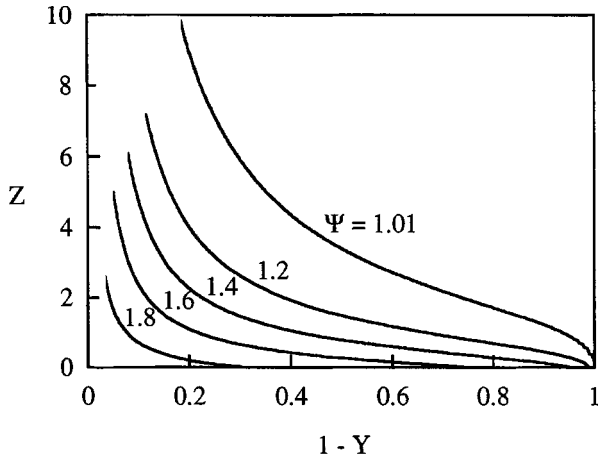

Figure 3. Contours of constant concentration computed for $\alpha_0 = 1$ and $\beta = 0.5$.

there was a rapid increase in thickness near the outer edge of the membrane, a slow increase at intermediate positions, and then another rapid increase near the center of the cell. The initial increase and tendency to level off are typical of boundary layers developing along surfaces (such as for flow parallel to a flat plate), whereas the final increase is due to the upward axial velocities that become dominant as the axis of rotation is approached. The plumelike behavior of the concentration field near the center of a stirred cell was examined in some detail by Smith and Colton (1972). As already mentioned, numerical instabilities precluded the calculation of the concentration field all the way to $Y = 1$. The size of the unstable region varied from the inner 3% of the cell radius at the membrane ($Z = 0$) to about the inner 20% of the cell radius at $Z = 10$, as indicated by the termination of the contours in Figure 3. For these conditions the product of dimensionless filtration rate (α) and dimensionless boundary-layer thickness (Z for $\Psi = 1.01$) was 0 at $Y = 0$, 0.84 at $Y = 0.4$, and 1.24 at $Y = 0.8$. This indicates that the similarity transformation of Saksena and Zydney (1997), which requires that product to be constant, would not have been applicable.

Effect of polarization on filtrate rate

The next set of simulations illustrates the effects of concentration polarization on the filtration rate averaged over the membrane surface. As with the calculations for Figure 3, it was assumed for simplicity that the membrane was perfectly semipermeable and the solution was ideal. The results were expressed by dividing the area-averaged filtration rate by that which would exist if polarization were absent. Thus, the quantity examined was

$$\frac{\langle v_f \rangle}{v_{f_0}} = \frac{\Delta P - \langle \Pi_m \rangle}{\Delta P - \Pi_b}, \tag{39}$$

where the brackets denote averages over membrane area and $\Pi_m = \Pi(C_m) = \Pi[C(r,0)]$. This relative filtration rate is plotted in Figure 4 as a function of α_0, for several values of β. As indicated by the solid curves, increasing α_0 at constant β decreased the relative filtration rate, because concentration polarization was enhanced. At a given α_0, increasing β also decreased the relative filtration rate, because it amplified the effects of osmotic pressure and thereby allowed polarization to play a greater role. For $\beta \to 0$ (applied pressure much greater than the osmotic pressure), polarization would be irrelevant, and the relative filtration rate would remain at unity for all values of α_0.

The dashed curves in Figure 4 represent predictions based on the stagnant-film theory. To obtain these curves, we interpreted all stagnant-film variables as area averages. Setting $C_m = \langle C_m \rangle$ and $v_f = \langle v_f \rangle$, and using $C_f = 0$ and $\Pi \propto C$ as before, Eq. 1 becomes

$$\frac{\langle \Pi_m \rangle}{\Pi_b} = \exp\left(\frac{\langle v_f \rangle}{k_{sf}}\right) = B. \tag{40}$$

To evaluate k_{sf} in Eq. 40 in a self-consistent manner, we used the area-averaged mass-transfer coefficient calculated using the boundary-layer model, in the limit of vanishing filtration rate. In other words, as might be attempted in practice, k_{sf} was obtained using mass-transfer data from the same system in the absence of filtration. The area-averaged mass-transfer coefficient was calculated using the results for $\alpha \to 0$ in Figure 2. In doing so the mass-transfer coefficient for $Y < 0.1$ was calculated from the similarity expression (Eq. 35). The result was

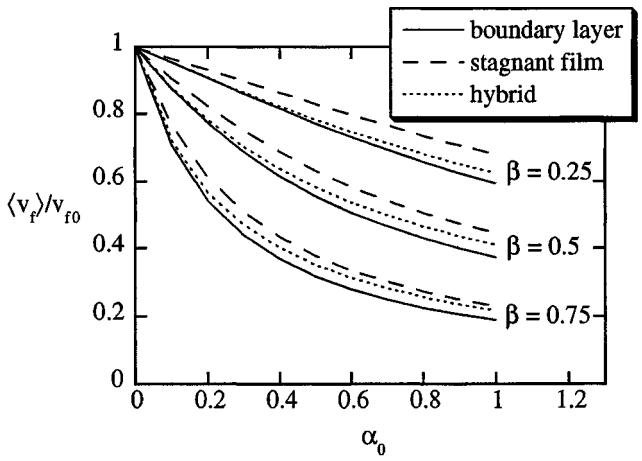

Figure 4. Ratio of average filtration rate to that in the absence of concentration polarization, as a function of the dimensionless filtration rate without polarization (α_0), for the boundary layer, stagnant film, and hybrid models.

The results are for an ideal semipermeable membrane.

$$\langle Sh \rangle = \frac{\langle k \rangle R}{D} = 1.01\, Re^{1/2} Sc^{1/3}. \tag{41}$$

If k_{sf} is set equal to $\langle k \rangle$, Eq. 40 becomes

$$\frac{\langle \Pi_m \rangle}{\Delta P} = \beta \exp\left[\frac{\alpha_0}{1.01(1-\beta)}\left(1 - \frac{\langle \Pi_m \rangle}{\Delta P}\right)\right]. \tag{42}$$

Equation 42 was solved iteratively to determine $\langle \Pi_m \rangle / \Delta P$. This allowed direct comparisons to be made between the stagnant film and boundary-layer results. As seen in Figure 4, the relative filtration velocity predicted by the stagnant-film model exceeded that obtained from the more rigorous boundary-layer theory for all values of α_0 and β. In other words, the stagnant-film approach always underestimated the effects of concentration polarization on filtration velocity. However, the difference between the two predictions was moderate, the stagnant film value being at most 21% higher than that from the boundary-layer theory. Similar trends were observed when the osmotic pressure was assumed to be a quadratic function of solute concentration. That is, it appears that in stirred cells there is always an overestimation of filtration rate by the stagnant film model, whether or not the solution is thermodynamically ideal.

The dotted curves in Figure 4 were obtained from a hybrid model, which was derived as follows. Letting $g(Y) = \Pi_m / \Pi_b$, the assumptions of an ideal semipermeable membrane and

ideal solution lead to

$$\frac{\langle v_f \rangle}{v_{f0}} = \frac{1-\langle g \rangle \beta}{1-\beta} \tag{43}$$

$$\langle g \rangle = 2\int_0^1 g(Y)(1-Y)\,dY. \tag{44}$$

Assuming that the stagnant-film result (Eq. 1) is valid locally, and interpreting k_{sf} now as the local mass-transfer coefficient in the absence of filtration, we obtain

$$g = \exp\left[\frac{\alpha_0}{f(Y,0)}\left(\frac{1-g\beta}{1-\beta}\right)\right]. \tag{45}$$

Using the results in Figure 2 to evaluate $f(Y,0)$, Eq. 45 was solved iteratively to determine $g(Y)$, from which the average filtration velocity was found. The difference between the numerically determined mass-transfer coefficient and the similarity result was approximately linear in Y, and a least-squares fit to the numerical results gave

$$f(Y,0) \cong 0.6381Y^{-1/3} - 0.410Y. \tag{46}$$

Equation 46 is sufficiently accurate that, when integrated to compute $\langle Sh \rangle$, it gives the correct value of 1.01 for the coefficient in Eq. 41. As shown in Figure 4, the hybrid model yielded predictions that were somewhat more accurate than those of the stagnant-film model, although it too consistently overestimated the relative filtration velocity. For the hybrid model, the maximum deviation from the boundary-layer results in Figure 4 was 15%.

Effect of polarization on sieving

The objective of the next set of simulations was to determine the relationship between the apparent sieving coefficient ($\Theta' = C_f/C_b$) and the actual sieving coefficient ($\Theta = C_f/C_m$), as a function of filtration conditions. As discussed in connection with Eq. 20, Θ was regarded as a constant. What is ordinarily measured is the concentration in the mixed filtrate divided by that in the bulk retentate, or $\langle \Theta' \rangle = \langle v_f C_f / v_f \rangle C_b$. However, in the simulations to be discussed the osmotic pressure was assumed to be negligible ($\beta \to 0$), making the filtration velocity independent of radial position. That is, the macromolecule solutions were assumed to be dilute, as is the case in membrane characterization experiments using tracers. Consequently, the apparent sieving coefficient could be calculated simply as $\langle \Theta' \rangle = \langle C_f \rangle / C_b$. Figure 5 shows the ratio of actual to apparent sieving coefficient as a function of the dimensionless filtrate rate (α), for values of Θ ranging from 0.01 to 0.75. The results for $\Theta = 0.01$ represent lower limits, in that they were indistinguishable on this plot from those for $\Theta = 0.001$. The boundary-layer results are shown by the solid curves. As the filtration rate was increased at a given value of Θ, polarization was augmented and $\Theta/\langle \Theta' \rangle (= C_b/\langle C_m \rangle)$ fell more and more below unity. At a given filtration rate, smaller values of Θ resulted in larger percentage differences between the apparent and actual sieving coefficient. In other words, the more effectively the solute is retained by the membrane, the greater is the influence of polarization on sieving.

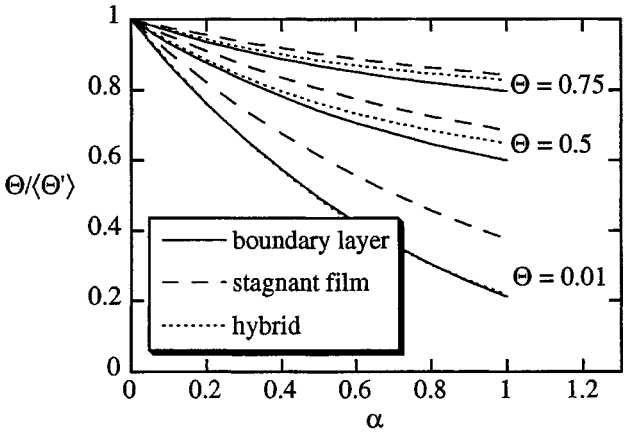

Figure 5. Ratio of actual sieving coefficient (Θ) to apparent sieving coefficient ($\langle \Theta' \rangle$) as a function of dimensionless filtration rate (α), for the boundary layer, stagnant film, and hybrid models.

The effects of osmotic pressure were neglected ($\beta = 0$).

To obtain comparable sieving predictions from the stagnant-film theory, we rearranged Eq. 1 to give

$$\frac{\Theta'}{\Theta} = \frac{B}{1-\Theta(1-B)} \tag{47}$$

and assumed that $\Theta' = \langle \Theta' \rangle$ and $B = \exp(\langle v_f \rangle / \langle k \rangle)$. As shown by the dashed curves in Figure 5, the values of $\Theta/\langle \Theta' \rangle$ from the stagnant-film model always exceeded those from the boundary-layer theory. The magnitude of this overestimate increased with increasing filtration rate or with decreasing sieving coefficient. At $\alpha = 1$ and $\Theta = 0.01$, the stagnant-film prediction for $\Theta/\langle \Theta' \rangle$ was 78% too large. Thus, using the stagnant-film model to correct measured (apparent) sieving coefficients can lead to systematic errors that are much larger than those made in estimating filtration rates.

The corresponding hybrid model was derived by using the local values of v_f and k to evaluate the polarization factor. From Eqs. 1 and 46, we obtain

$$B(Y) \equiv \frac{C_m(Y) - C_f(Y)}{C_b - C_f(Y)} = \exp\left[\frac{\alpha}{0.6381Y^{-1/3} - 0.410Y}\right]. \tag{48}$$

Averaging Eq. 47 over the membrane surface then gives

$$\frac{\langle \Theta' \rangle}{\Theta} = 2\int_0^1 \frac{B(Y)(1-Y)}{1-\Theta[1-B(Y)]}\,dY. \tag{49}$$

As shown by the dotted curves in Figure 5, the predictions of the hybrid model were significantly more accurate than those of the stagnant-film approach. A particularly dramatic improvement was seen for very small sieving coefficients (such as $\Theta = 0.01$). For the hybrid model, the maximum deviation from the boundary-layer results was 15% for $\Theta = 0.1-0.2$).

For the stagnant-film calculations presented in Figures 4 and 5 it was assumed that $k_{sf} = \langle k \rangle$, with $\langle k \rangle$ evaluated from

Eq. 41. This provided the most natural basis for comparing the models, because the mass-transfer coefficient averaged over a surface is often measurable, and because Eq. 41 provides the correct limiting value of $\langle k \rangle$ as the filtration velocity approaches zero. As mentioned in connection with Eq. 33, a vanishing filtration velocity corresponds to a constant concentration gradient at the membrane surface. Because measurements of $\langle k \rangle$ in a stirred cell might be made instead under conditions of constant surface concentration, we tested the effect of altering the mass-transfer coefficient in that manner. For a constant concentration boundary condition, the only change in the expression for the average Sherwood number (Eq. 41) is that the numerical coefficient is reduced from 1.01 to 0.775. When this lower value of $\langle k \rangle$ was used, the extent of polarization calculated with the stagnant-film model increased somewhat, making the results more accurate; the maximum errors were then 2% and 33% for the conditions of Figures 4 and 5, respectively. Similarly reduced errors were obtained if it was assumed that $k_{sf} = 1/\langle k^{-1} \rangle$, with the local value of k evaluated once again under constant gradient conditions. Because the local film thickness is proportional to k^{-1}, this last approach is equivalent to averaging the film thickness over the surface, rather than averaging the mass-transfer coefficient. This last observation may have little practical value, in that we are unaware of any way to measure $\langle k^{-1} \rangle$.

Comparisons with experimental data

The predictive capability of the boundary-layer model was tested by applying it to filtration data for 4% (w/v) BSA solutions reported previously (Johnston and Deen, 1999). Briefly, regenerated cellulose membranes with a molecular weight cutoff of 30 kD were used in commercially available stirred cells of 3 mL or 10 mL capacity. Scale drawings of the two cells are shown in Figure 6. In all experiments the angular velocity of the impeller was maintained at 220 rpm, resulting in Reynolds numbers (based on ω_s) of approximately 880 and 2690 for the 3-mL and 10-mL cells, respectively. Nearly perfect rejection of the 68-kD BSA was observed ($\langle \Theta' \rangle \cong 10^{-3}$), so the membranes were modeled as ideally semipermeable. The osmotic pressure was related to the BSA concentration using the following semiempirical correlation (Vilker et al., 1981):

$$\Pi_{\mathrm{BSA}} = RT\left\{2\left[\left(\frac{zC_{\mathrm{BSA}}}{2M_{\mathrm{BSA}}}\right)^2 + m_s^2\right]^{1/2} - 2m_s\right\} + \frac{RT}{M_{\mathrm{BSA}}}\left(C_{\mathrm{BSA}} + A_2C_{\mathrm{BSA}}^2 + A_3C_{\mathrm{BSA}}^3\right), \quad (50)$$

where z is the charge number for BSA, C_{BSA} is the BSA concentration in g/L, M_{BSA} is the molecular weight of BSA, m_s is the molar salt concentration, and A_2 and A_3 are constant coefficients. Filtration rates were measured with protein-free salt solutions and with 4 g/dL BSA, at various levels of ΔP.

The predicted and measured filtration rates for the 10-mL cell are compared in Figure 7. Values of β for this data set ranged from 0.37 to 0.66; values of α calculated using ω_s ranged from 0.07 to 0.27. When the angular velocity of the bulk fluid was equated with that of the stirrer ($\gamma \equiv \omega/\omega_s = 1$), the filtration rates predicted by the model exceeded the measured values by approximately 20%. As mentioned earlier, however, to impart a torque that will balance those exerted on the fluid by the bottom and side of the cell, the angular velocity of the stirrer must exceed that of the bulk fluid. In other words, we expect that $\gamma < 1$. As shown in Figure 7, when it was assumed that $\gamma = 0.25$, the predicted filtration rates underestimated the measured values, whereas $\gamma = 0.36$ was found to minimize the sum of the squared errors. Colton and Smith (1972) measured the rate of benzoic acid dissolution from the base of a different stirred cell and compared the results with boundary-layer predictions for a constant con-

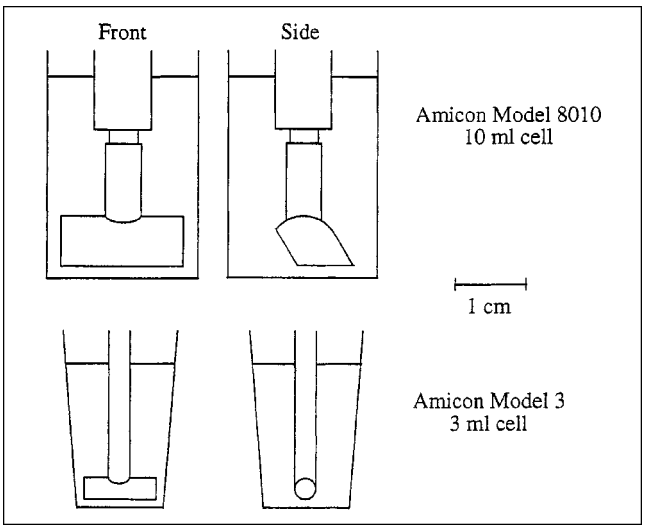

Figure 6. Amicon stirred cells used in the filtration experiments with BSA.

The fluid levels indicated correspond to the nominal capacities. The values of R and the impeller–membrane separation were 1.05 and 0.14–0.18 cm, respectively, for the 10-mL cell, and 0.6 and 0.10 cm, respectively, for the 3-mL cell.

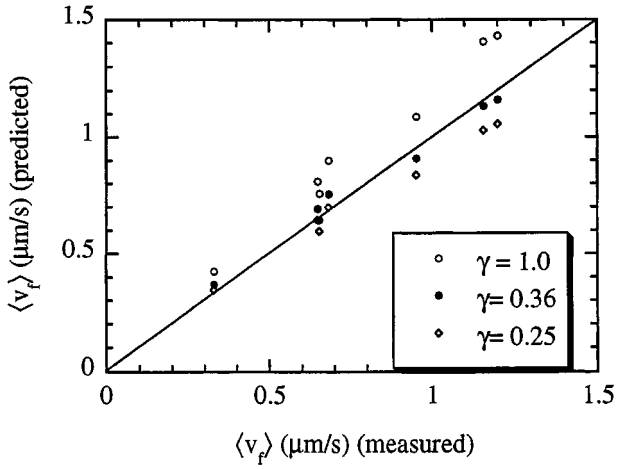

Figure 7. Comparison of average filtration rates predicted by the boundary-layer model with those measured in the 10-mL cell.

Predictions are shown for three assumed values of $\gamma = \omega/\omega_s$; the best-fit value was $\gamma = 0.36$.

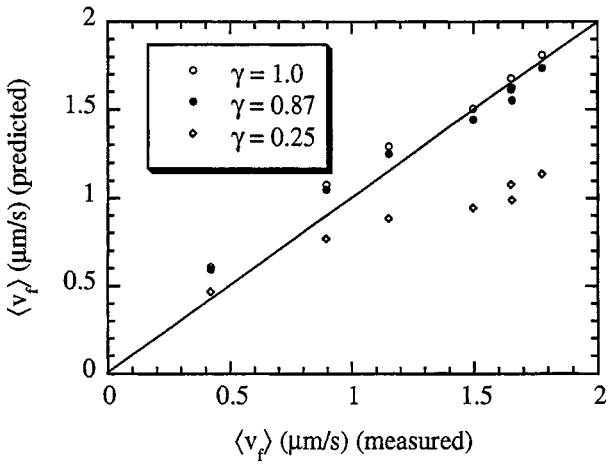

Figure 8. Comparison of average filtration rates predicted by the boundary-layer model with those measured in the 3-mL cell.

Predictions are shown for three assumed values of $\gamma = \omega/\omega_s$; the best-fit value was $\gamma = 0.87$.a

centration boundary condition, thereby concluding that $\gamma = 0.49$. Inasmuch as γ must depend on the cell and impeller geometry, this difference in angular velocity factors is not surprising.

The results for the 3-mL cell, where the best-fit value was $\gamma = 0.87$, are shown in Figure 8. Values of β for this data set were similar to those for the 10-mL cell, ranging from 0.39 to 0.62. Values of α, calculated using ω_s, were also similar (0.06–0.26). However, in this case the agreement between the model and data was somewhat less satisfactory than for the 10-mL cell. In particular, for the 3-mL cell a fixed value of γ did not match the data equally well over the entire range of filtration rates, larger values of γ tending to work better at the higher filtration rates. Possibly contributing to this trend is the fact that the mean fluid heights were significantly lower at the higher values of $\langle v_f \rangle$, due to the small volume of this cell. By reducing the wetted area, this would have lowered the torque exerted on the fluid by the side of the cell, and thereby reduced the value of $\omega_s - \omega$ needed to balance that torque. A reduction in $\omega_s - \omega$ corresponds, of course, to values of γ closer to unity.

We have shown previously (Johnston and Deen, 1999) that the stagnant-film model can be fitted to the BSA data if k_{sf} is allowed to be a function of the filtration rate. The results for both ultrafiltration cells are represented accurately by assuming that $k_{sf} = 1.36 + 2.40\langle v_f \rangle$, where the units of k_{sf} and $\langle v_f \rangle$ are μm/s. However, the results from the boundary-layer model indicate that the true area-average mass-transfer coefficients are not strongly dependent on the filtration rate. For example, doubling the filtration rate in the boundary-layer model from 0.5 to 1 μm/s resulted in less than a 5% change in the value of $\langle k \rangle$ predicted for the conditions of the BSA experiments, whereas the empirical expression for k_{sf} yields nearly a 50% increase. Evidently, most of the empirical dependence of k_{sf} on $\langle v_f \rangle$ is needed merely to compensate for errors that result from the use of Eq. 1.

The fact that the hybrid model gave noticeably better predictions of filtration rates (Figure 4) and sieving coefficients (Figure 5) indicates that a significant source of error in the stagnant-film approach is the use of area averages for the various individual quantities in Eq. 1. Indeed, the distinguishing feature of the hybrid model is that the necessary averaging is done rigorously. The fact that there are residual errors with the hybrid model suggests that there is something else wrong with the stagnant-film approach, namely, that Eq. 1 is not precisely correct, even locally. That is, contrary to the predictions of the one-dimensional model that underlies Eq. 1, the solute concentration is not exactly an exponential function of z.

In practice, the empirical parameter in the stagnant-film model (e.g., k_{sf}) is often estimated from filtration data obtained with a fully retentive membrane, and that parameter value is then used to correct sieving coefficients measured in the same stirred cell with a partially permeable membrane (e.g., Opong and Zydney, 1991; Johnston and Deen, 1999). When the stagnant-film model is used in this manner, to what extent will its errors cancel? This question was addressed by treating the boundary-layer predictions in Figures 4 and 5 as the "data," and applying the stagnant-film model to those results. It proved to be most convenient to regard the polarization factor, B, as the empirical parameter. For a given solute, stirring rate, and cell geometry, it was assumed that in the filtration experiments B would depend only on the filtrate velocity (as expressed by α, not α_0) and the relative osmotic pressure (β). Accordingly, the boundary-layer results for $\langle v_f \rangle / v_{f0}$ in Figure 4 were used to compute B for some 33 combinations of α and β, using Eq. 40. Apparent sieving coefficients were then calculated for various combinations of α and Θ, using Eq. 47. Figure 9 compares the sieving coefficients predicted by the stagnant-film model with the "exact" values obtained from the boundary-layer theory. The agreement was excellent in all cases. We conclude that there will be minimal error in using the stagnant-film model to correct sieving coefficients for polarization, provided that care is

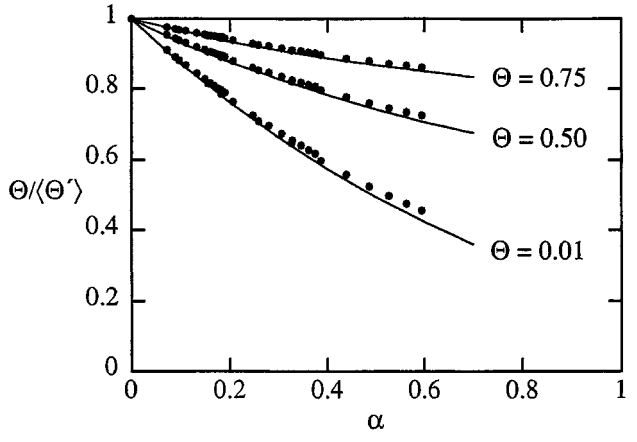

Figure 9. Ratio of actual sieving coefficient (Θ) to apparent sieving coefficient ($\langle \Theta' \rangle$) as a function of dimensionless filtration rate (α), for the boundary-layer and stagnant-film models.

The boundary-layer results, which are repeated from Figure 5, are shown by the continuous curves. The symbols represent stagnant-film predictions obtained by first fitting the value of the polarization parameter to the filtration data in Figure 4, as described in the text.

taken to evaluate the empirical parameter at the same filtrate velocity as in the sieving experiments. In other words, the values of α must be matched, as was done in computing the results in Figure 9. The need to match filtrate velocities is underscored by the strong dependence of k_{sf} on $\langle v_f \rangle$ in the data of Johnston and Deen (1999), as discussed earlier. Solutes of similar size should also be used in the two experiments, because the stagnant-film model does not properly account for differences in diffusivity.

Conclusions

A laminar boundary-layer analysis based on Bödewadt flow was used to quantify concentration polarization in stirred, cylindrical ultrafiltration cells. The predictive capability of the boundary-layer model was tested using previously reported filtration data with BSA solutions, and the agreement was found to be excellent, provided that an appropriate value was selected for the angular velocity of the bulk fluid. Comparisons of the boundary-layer results with those obtained from a conventional stagnant-film model showed that the latter gave moderately accurate values for mean filtrate velocities, but made substantial errors in converting apparent sieving coefficients to actual membrane sieving coefficients. The errors were lessened by use of a hybrid model, where the mass-transfer coefficient was allowed to vary with position, according to boundary-layer theory. The problems with the stagnant-film approach were found to arise both from its implicit averaging of concentrations and filtrate velocities over the membrane surface, and from its imperfect approximation to the local concentration profile. Of course, the use of quantities that are independent of position on the membrane is what was needed to yield a one-dimensional problem with a simple analytical solution. We conclude that the one-dimensional nature of the stagnant-film model, which is its main strength, is also its main weakness.

Acknowledgment

This work was supported by Grant DK 20368 from the National Institutes of Health.

Literature Cited

Battacharjee, S., A. S. Kim, and M. Elimelech, ''Concentration Polarization of Interacting Solute Particles in Cross-Flow Membrane Filtration,'' *J. Colloid Interface Sci*., **212**, 81 (1999).

Blatt, W. F., A. Dravid, A. S. Michaels, and L. Nelsen, ''Solute Polarization and Cake Formation in Membrane Ultrafiltration,'' *Membrane Science and Technology*, J. E. Flinn, ed., Plenum Press, New York (1970).

Colton, C. K., and K. A. Smith, ''Mass Transfer to a Rotating Fluid: Part II. Transport from the Base of an Agitated Cylindrical Tank,'' *AIChE J*., **18**, 958 (1972).

Deen, W. M., *Analysis of Transport Phenomena*, Oxford Univ. Press, New York (1998).

Denisov, G. A., ''Theory of Concentration Polarization in Cross-Flow Ultrafiltration: Gel-Layer Model and Osmotic-Pressure Model,'' *J. Memb. Sci*., **91**, 173 (1994).

Gill, W. N., D. E. Wiley, C. J. D. Fell, and A. G. Fane, ''Effect of Viscosity on Concentration Polarization in Ultrafiltration,'' *AIChE J*., **34**, 1563 (1988).

Johnston, S. T., and W. M. Deen, ''Hindered Convection of Proteins in Agarose Gels,'' *J. Memb. Sci*., **153**, 271 (1999).

Kozinski, A. A., and E. N. Lightfoot, ''Ultrafiltration of Proteins in Stagnation Flow,'' *AIChE J*., **17**, 81 (1971).

Madireddi, K., R. B. Babcock, B. Levine, J. H. Kim, and M. K. Stenstrom, ''An Unsteady-State Model to Predict Concentration Polarization in Commercial Spiral Wound Membranes,'' *J. Memb. Sci*., **157**, 13 (1999).

Michaels, A. S., ''New Separation Technique for the CPI,'' *Chem. Eng. Prog*., **64**, 31 (1968).

Opong, W. S., and A. L. Zydney, ''Diffusive and Convective Protein Transport Through Asymmetric Membranes,'' *AIChE J*., **37**, 1497 (1991).

Rogers, M. H., and G. N. Lance, ''The Rotationally Symmetric Flow of a Viscous-Fluid in the Presence of an Infinite Rotating Disk,'' *J. Fluid Mech*., **7**, 617 (1960).

Saksena, S., and A. L. Zydney, ''Influence of Protein-Protein Interactions on Bulk Mass Transport During Ultrafiltration,'' *J. Memb. Sci*., **125**, 93 (1997).

Schlichting, H., *Boundary Layer Theory*, 7th ed., McGraw-Hill, New York (1979).

Sherwood, T. K., P. L. T. Brian, R. E. Fisher, and L. Dresner, ''Salt Concentration at Phase Boundaries in Desalination by Reverse Osmosis,'' *Ind. Eng. Chem. Fundam*., **4**, 113 (1965).

Shen, J. J. S., and R. F. Probstein, ''On the Prediction of Limiting Flux in Laminar Ultrafiltration of Macromolecular Solutions,'' *Ind. Eng. Chem. Fundam*., **16**, 459 (1977).

Smith, K. A., and C. K. Colton, ''Mass Transfer to a Rotating Fluid: Part I. Transport from a Stationary Disk to a Fluid in Bödewadt Flow,'' *AIChE J*., **18**, 949 (1972).

Vilker, V. L., C. K. Colton, and K. A. Smith, ''The Osmotic Pressure of Concentrated Protein Solutions: Effect of Concentration and pH in Saline Solutions of Bovine Serum Albumin,'' *J. Colloid Interface Sci*., **79**, 548 (1981).

Zydney, A. L., ''Stagnant Film Model for Concentration Polarization in Membrane Systems,'' *J. Memb. Sci*., **130**, 275 (1997).

Manuscript received Nov. 18, 1999, and revision received Aug. 14, 2000.